Improved Core-Loss Calculation for Magnetic Components Employed in Power Electronic Systems

Jonas Mühlethaler, *Student Member, IEEE*, Jürgen Biela, *Member, IEEE*, Johann Walter Kolar, *Fellow, IEEE*, and Andreas Ecklebe, *Member, IEEE*

***Abstract*—In modern power electronic systems, voltages across inductors or transformers generally show rectangular shapes, including periods of zero voltage. In the stage of zero applied voltage (constant flux), core losses are not necessarily zero. At the beginning of a period of constant flux, losses still occur in the material. This is due to relaxation processes. A physical explanation about magnetic relaxation is given and a new core-loss modeling approach that takes relaxation effects into consideration is introduced. The new loss model is called improved-improved generalized Steinmetz equation ($\mathrm{i^2GSE}$) and it has been verified experimentally.**

***Index Terms*—Core losses, dual active bridge (DAB), ferrite, relaxation, Steinmetz.**

I. Introduction

IN MODERN power electronic systems, voltages across inductors or transformers generally show rectangular shapes as illustrated in Fig. 1. The voltage across an inductor or transformer can be positive, negative, or zero. This results in the flux in the core ramping up, ramping down, or remaining constant.

Core losses need to be determined for the design of inductive components. The most used equation that characterizes core losses is the power equation [1]

$$P_\mathrm{v} = k f^\alpha \hat{B}^\beta \tag{1}$$

where $\hat{B}$ is the peak induction of a sinusoidal excitation with frequency f; P_v is the time-average power loss per unit volume; and k, α, and β are material parameters. The equation is called the Steinmetz equation (after Charles P. Steinmetz). The material parameters k, α, and β are accordingly referred to as the Steinmetz parameters. They are valid for a limited frequency and flux density range. The major drawback of the Steinmetz equation is that it is only valid for sinusoidal excitation. This is a huge drawback, because, as stated earlier, in power electronic applications, the material is usually exposed to nonsinusoidal flux waveforms.

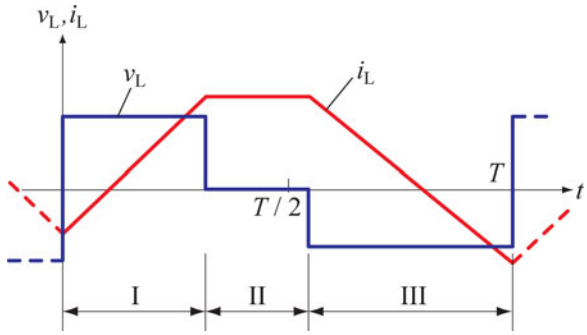

Fig. 1. Typical voltage/current waveform of magnetic components employed in power electronic systems. Phase I: positive voltage. Phase II: zero voltage. Phase III: negative voltage.

To overcome this limitation and determine losses for a wider variety of waveforms, different approaches have been developed. The approaches can be classified into the following categories.

1) Improvements of the Steinmetz equation (1): for instance, the analysis in [2] is motivated by the fact that the loss due to domain wall motion has a direct dependence of $\mathrm{d}B/\mathrm{d}t$. As a result, a modified Steinmetz equation is proposed. In [3], the approach is further improved, and in [4], a method on how to deal with minor hysteresis loops is presented and some minor changes on the equation are made. The approach of [2]–[4] leads to the improved generalized Steinmetz equation (iGSE)

$$P_\mathrm{v} = \frac{1}{T}\int_0^T k_i \left|\frac{\mathrm{d}B}{\mathrm{d}t}\right|^\alpha (\Delta B)^{\beta-\alpha}\,\mathrm{d}t \tag{2}$$

where ΔB is peak-to-peak flux density and

$$k_i = \frac{k}{(2\pi)^{\alpha-1}\int_0^{2\pi} |\cos\theta|^\alpha 2^{\beta-\alpha}\mathrm{d}\theta}. \tag{3}$$

The parameters k, α, and β are the same parameters as used in the Steinmetz equation (1). By the use of the iGSE, losses of any flux waveform can be calculated, without requiring extra characterization of material parameters beyond those for the Steinmetz equation. This approach is widely applied [5], [6].

2) Calculation of the losses with a loss map that is based on measurements. This loss map stores the loss information for different operating points, each described by the flux

Manuscript received March 16, 2011; revised May 19, 2011 and June 28, 2011; accepted July 7, 2011. Date of current version January 9, 2012. Recommended for publication by Associate Editor C. R. Sullivan.

J. Mühlethaler and J. W. Kolar are with the Power Electronic Systems Laboratory, Zurich CH-8092, Switzerland (e-mail: muehlethaler@lem.ee.ethz.ch; kolar@lem.ee.ethz.ch).

J. Biela is with the Laboratory for High Power Electronic Systems, Swiss Federal Institute of Technology (ETH) Zürich, Zurich CH-8092, Switzerland (e-mail: jbiela@ethz.ch).

A. Ecklebe is with ABB Switzerland Ltd., Corporate Research, Baden-Dättwil CH-5405, Switzerland (e-mail: andreas.ecklebe@ch.abb.com).

Color versions of one or more of the figures in this paper are available online at http://ieeexplore.ieee.org.

Digital Object Identifier 10.1109/TPEL.2011.2162252

density ripple ΔB, the frequency f, the temperature T, and a dc bias H_{dc} (e.g., in [7]–[9]).

3) Methods to determine core losses based on breaking up the total loss into loss components, i.e., hysteresis losses, classical eddy-current losses, and residual losses [10], [11].
4) Hysteresis models, such as Preisach model and Jiles–Atherton model, used for calculating core losses.

In categories 1 and 2, an energy loss is assigned to each section of the voltage/current waveform as illustrated in Fig. 1 (e.g., via an equation as (2) or via a loss map), and these losses are summed up to calculate the power loss occurring in the core. This approach has, e.g., been implemented in [12].

In most of the previous publications, the phase where the voltage across the magnetic component is zero has not been discussed. It has been implicitly assumed that no losses occur when the flux remains constant. However, as measurements show, this is not a valid simplification. At the beginning of a period of constant flux, losses still occur in the material. In the publication [13] about core-loss modeling, a loss increase during zero-voltage periods has been observed; however, no explanation or modeling approach is given.

This study hypothesizes that this loss increase is due to relaxation processes in the magnetic core material. In accordance with this hypothesis, a new model is proposed that considers relaxation processes when calculating core losses.

A core-loss measurement test setup has been built to analyze core losses under general flux waveform excitations. The test system is presented in Section II. In Section III, a brief introduction to magnetic relaxation is given. In Sections IV–VI, a new loss model is derived that substantially improves core-loss calculation by taking relaxation processes into consideration. In Section VII, an easy-to-follow example is given to illustrate how the new model can be applied. Before concluding this study, in Section VIII, a short discussion of the behavior of different materials is given.

II. Test Setup to Measure Core Losses

In order to perform core-loss measurements, the best measurement technique has to be selected first. In [14], different methods are compared. The *B–H* loop measurement has been evaluated as the most suitable. Among other advantages, this technique offers rapid measurement (compared to other methods, e.g., calorimetric measurements) and a good accuracy. Furthermore, copper losses are excluded from the measurement. The principle is as follows: two windings are placed around the core under test (CUT). The sense winding (secondary winding) voltage v is integrated to sense the core flux density B

$$B(t) = \frac{1}{N_2 \cdot A_{\mathrm{e}}} \int_0^t v(\tau)\mathrm{d}\tau \tag{4}$$

where N_2 is the number of sense winding turns and A_{e} is the effective core cross section of the CUT. The current in the excitation winding (primary winding) is proportional to the magnetic field strength H

$$H(t) = \frac{N_1 \cdot i(t)}{l_{\mathrm{e}}} \tag{5}$$

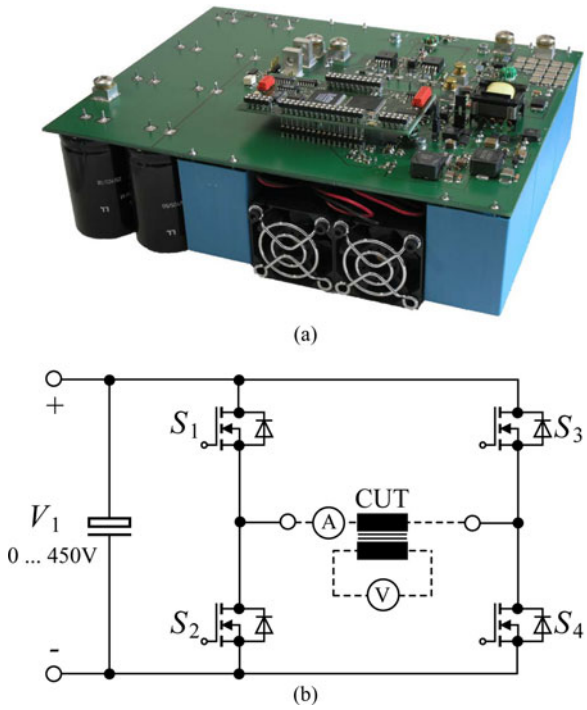

Fig. 2. Test setup (a) photograph and (b) simplified schematic.

where N_1 is the number of excitation winding turns and l_{e} is the effective magnetic path length of the CUT. The loss per unit volume is then the enclosed area of the *B–H* loop multiplied by the frequency f:

$$\frac{P}{V} = f \oint H\mathrm{d}B. \tag{6}$$

The selected approach is widely used [4], [8], [15], [16]. The built test system consists of a power stage, a power supply, an oscilloscope, and a heating chamber. It is controlled by a MATLAB program running on the oscilloscope under Microsoft Windows. In Fig. 2(a) and (b), a photograph and the simplified schematic of the power stage are shown. The power stage is capable of a maximum input voltage of $450\,\mathrm{V}$, output current of $25\,\mathrm{A}$, and a switching frequency of up to $200\,\mathrm{kHz}$. The test setup allows application of a general rectangular voltage shape across the CUT that leads to a triangular or trapezoidal current shape including a dc bias (if desired).

See [17] for more information about the test setup, including a detailed accuracy analysis of the loss measurement.

III. Relaxation Processes in Magnetic Materials

As mentioned in Section I, during the phase of constant flux (where the voltage across the magnetic component is zero) losses still occur in the core material. A literature survey led to the conclusion that this is due to relaxation processes in the magnetic core material. In this section, first measurements are presented that illustrate magnetic relaxation. Then, an attempt to theoretically explain the effect is given and, with it, the resulting shape of a *B–H* loop for trapezoidal flux waveform is analyzed.

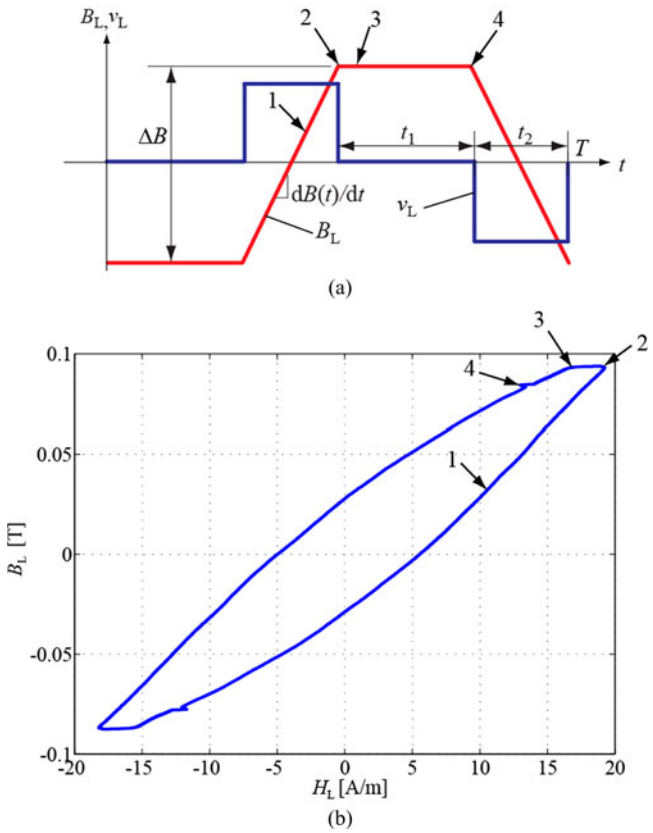

Fig. 3. (a) Voltage and flux density waveforms. (b) *B–H* loop to illustrate magnetic relaxation under trapezoidal flux shape condition.

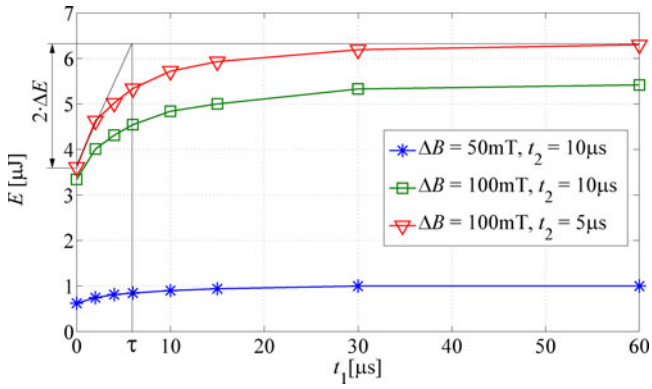

Fig. 4. Measurement results measured on ferrite EPCOS N87 (R42, B64290L22X87 [18]); temperature $= 25\,^{\circ}\mathrm{C}$. It is further illustrated how τ according to (18) can be extracted.

A. Measurement Results

According to (2), the energy loss would only depend on the magnitude and the slope of the flux, and consequently, there should be no loss during periods of constant flux (zero voltage). Measurements on waveforms as illustrated in Fig. 3(a) have been performed to investigate this. Fig. 4 shows the corresponding measurement results. The CUT is made of ferrite EPCOS N87 (size R42). According to (2), the duration of t_1 should not influence the *energy* loss per cycle, but, as can be seen, increasing t_1 has a substantial influence on the energy loss per cycle. In particular, a change in t_1 at low values of t_1 influences the dissipated loss. For larger values of t_1, the core material has time to reach its equilibrium state and no increase in losses can be observed when t_1 is further increased.

Different experiments have been conducted to confirm that this effect is not due to an imperfection of the measurement setup. The main thinkable sources of error include:

1) The effect of a small exponential change of current due to a residual voltage across the inductor in the "zero" voltage time intervals, i.e., an effect related to the CUT excitation.
2) An error in measurements due to limited measurement capabilities of the probes, i.e., an effect related to the measurement equipment used.

The following experiments have been conducted to make sure that neither of these error sources led to the observed loss increase.

1) A resistor has been connected in series with the primary winding, i.e., the effect of an exponential change of the current due to a voltage drop across the inductor in the "zero" voltage time intervals has been deliberately increased. A resistor of $10\,\Omega$ has been chosen since this value is certainly higher than the residual resistance of the setup (for instance, the on-resistance of one MOSFET (IXYS IXFB82N60P) is only $R_{\mathrm{DS(on)}} = 75\,\mathrm{m}\Omega$ at $T_{\mathrm{j}} = 25\,^{\circ}\mathrm{C}$; $I_{\mathrm{D}} = 41\,\mathrm{A}$). The excitation voltage has been accordingly adjusted to have the same magnetic operating point. The same core-loss increase in the "zero" voltage time interval has been observed as without an additional resistor, which indicates that the effect is not coming from an improper CUT excitation.
2) The current probe LeCroy AP015 has, with 50 MHz, the lowest bandwidth of the measurement equipment used. This is enough to measure the effect observed in Fig. 4. Generally, according to the accuracy analysis in [17], accurate measurement results are expected for operating points with frequencies/flux densities, such as presented in Fig. 4. However, to confirm this, a simple comparative measurement has been performed to verify that the effect is not originating in the limitations of the voltage and current probes. For a limited temperature range, it can be approximated that the relative change of the core temperature is proportional to the losses occurring in the core. According to this, the core losses can be observed by measuring the core temperature. The same loss increase in the zero-voltage time intervals as illustrated in Fig. 4 could be observed by this simple measurement. This comparative measurement indicates that the effect is not coming from the measurement equipment used.

Last but not least, the fact that this effect has also been observed by another research group [13] greatly increases the credibility of the result.

In conclusion, at the beginning of the phase of constant flux (where the voltage across the magnetic component is zero) losses still occur. Based on a literature survey, it is hypothesized that this is because of relaxation processes in the magnetic

core material. Next, a brief introduction to magnetic relaxation is given.

B. Theory of Relaxation Effects

There are basically three physical loss sources: (static) hysteresis losses, eddy-current losses, and a third loss component, which is often referred to as residual losses. Hysteresis losses are linear with the frequency f (rate-independent *B–H* loop). Eddy-current losses occur because of an induced current due to the changing magnetic field and strongly depend on the material conductivity and the core geometry. The residual losses are, according to [10], due to relaxation processes: if the thermal equilibrium of a magnetic system changes, the system progressively moves toward the new thermal equilibrium condition. When the magnetization changes rapidly, as, for example, is the case in high-frequency or pulsed field applications, such relaxation processes become very important.

The *Landau–Lifshitz* equation describes qualitatively the dynamics of the magnetic relaxation processes. This is a phenomenological equation that combines all processes that are involved in magnetic relaxation. The equation follows directly from equating the rate of change of the angular momentum L to the torque $\mathbf{M} \times \mathbf{H}$ reduced by a frictional term that is directed opposite to the direction of motion [10]:

$$\frac{\mathrm{d}\mathbf{M}}{\mathrm{d}t} = \gamma \mathbf{M} \times \mathbf{H} - \Lambda \mathbf{M} \times (\mathbf{M} \times \mathbf{H})/M^2 \qquad (7)$$

where $\gamma = ge/2mc$ is the magnetomechanical ratio M/L; $\mathbf{M}$ is the magnetization vector; $\mathbf{H}$ the magnetic field vector, and Λ is called the relaxation frequency. It describes how the system progressively moves toward the new thermal equilibrium. The equilibrium is achieved by rearranging the magnetic domain structures to reach states of lower energy. The relaxation process limits the speed of flux change; hence, the *B–H* loops become rate dependent. Several physical processes are contributing simultaneously to magnetic relaxation. See [10], [19], and [20] for more information.

In conclusion, due to *magnetic relaxation*, the magnetization may change even when the applied field is constant (the magnetization is delayed). Consequently, a residual energy loss still occurs in the period of a constant applied field. Furthermore, the shape of the hysteresis loop is changed depending on the rate of change of the applied field (rate-dependent loop). An analysis of the impact of *magnetic relaxation* to a trapezoidal flux shape follows.

C. Shape of the B–H Loop for Trapezoidal Flux Waveforms

A *B–H* loop under the trapezoidal flux waveform condition has been measured to gain a better comprehension of why the losses increase when the duration of the zero-voltage period is increased. The CUT is a toroid core R42 made of ferrite EPCOS N87. In Fig. 3(a) and (b), the flux waveform and the corresponding *B–H* loop are plotted, respectively. The *B–H* loop always traverses counterclockwise. The different instants [see numbers in Fig. 3(a) and (b)] are now discussed step by step.

1) A constant voltage at the CUT primary winding results in a time linear flux increase.
2) The CUT primary voltage is set to zero; as a consequence, the flux is frozen ($\mathrm{d}B/\mathrm{d}t = 0$). However, the material has not yet reached its thermal equilibrium. The magnetic field strength H declines to move toward the new thermal equilibrium and, therewith, reaches a state of lower energy. This can also be observed in the current (the current declines accordingly).
3) This point is reached approximately $24\,\mu$s after point 2. It is the point of the new thermal equilibrium.
4) This point is reached approximately $200\,\mu$s after point 3. The demagnetization in the zero-voltage period is due to the small voltage drop over the on-resistance of the MOSFETs and copper resistance of the inductor primary winding. This demagnetization follows a different time constant than the demagnetization due to relaxation losses (the approximately same distance 2–3 and 3–4, but the different time scale). At point 4, a negative voltage is applied to the CUT. The small buckle in the *B–H* loop is due to small capacitive currents at the switching instant.

The period between points 2 and 3 obviously increases the area of the *B–H* loop and, therewith, increases the core losses. The loop area increases as a function of the duration t_1. After the thermal equilibrium is reached (in the aforementioned example after approximately $24\,\mu$s) the loss increase becomes (almost) zero. In the next section, more measurements are presented to find a method to include this effect into an existing core-loss model.

IV. Model Derivation 1: Trapezoidal Flux Waveform

Losses can be calculated with (2), without requiring extra characterization of material parameters beyond the parameters for the Steinmetz equation. The Steinmetz parameters are often given by core manufacturers; hence, core-loss modeling is possible without performing extensive measurements. However, the approach has some drawbacks. First, it neglects the fact that core losses may vary under the dc bias condition. This is discussed in [17], where a graph showing the dependence of the Steinmetz parameters (α, β and k) on premagnetization is introduced. With this, losses can be calculated via the Steinmetz equation (1) or the iGSE (2) using appropriate Steinmetz parameters. Another source of inaccuracy is that relaxation effects are not taken into consideration. As approach (2) is very often discussed in the literature and often applied for designing magnetic components, improving this method would have the most practical use. Furthermore, in [6], it has been evaluated as the most accurate state-of-the-art loss model based on Steinmetz parameters. For these two reasons, in the following discussion, the iGSE will be extended to consider relaxation losses as well.

When we plot the losses with logarithmic axes, where the x-axis represents the frequency and the y-axis represents the power loss, an approximately straight line is drawn. This is because the losses follow a power function as, e.g., the law stated in (1). The parameter α of (1) represents the slope of the curve in the plot. In Fig. 5, such plots are given for few operating points. Instead of

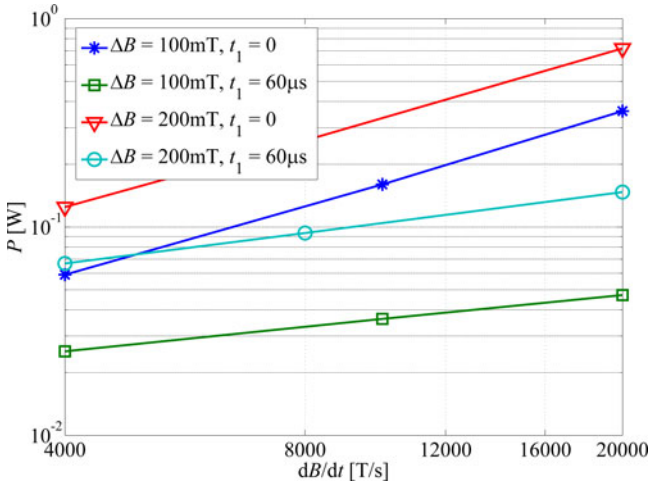

Fig. 5. Core loss (ferrite N87; measured on R42 core); temperature = 25 °C.

the frequency f, $\mathrm{d}B/dt$ has been used as the x-axis, which, for symmetric triangular or trapezoidal flux waveforms, is directly proportional to the frequency f. The time t_1 is defined as in Fig. 3 ($t_1 = 0$ leads to a triangular flux waveform). As can be seen in Fig. 5, when a long zero-voltage phase is added between two voltage pulses (having a flux waveform as given in Fig. 3), the loss still follows a power function with variable $\mathrm{d}B/\mathrm{d}t$ (the losses are still represented by an approximately straight line). The same conclusion can be made when keeping $\mathrm{d}B/\mathrm{d}t$ constant and varying ΔB; hence, the use of a power function with variable ΔB is justified as well.

It should be pointed out that when a (long) zero-voltage interval ($t_1 \neq 0$) is present the average power loss decreases (see Fig. 5). There is no discrepancy with the observation in Fig. 4, where an *energy loss per cycle* increase has been observed. When having a zero-voltage interval, the energy loss per cycle increases, but the period increases as well and leads to a lower average power loss.

The approach of (2) will now be extended by taking relaxation effects into consideration. This is done by adding a new additional term that represents the relaxation effect of a transition to zero voltage. As can be seen in Fig. 4, the energy-loss increase due to the zero-voltage interval can be modeled with the exponential equation

$$E = \Delta E \left(1 - e^{-\frac{t_1}{\tau}}\right) \tag{8}$$

where ΔE is the maximum energy-loss increase (which occurs when the magnetic material has enough time to reach the new thermal equilibrium), τ is the relaxation time that has to be further determined, and t_1 is the duration of the constant flux (zero applied voltage) phase. The exponential behavior is typical for relaxation processes. Measurements have shown that τ can be considered to be a constant parameter for a given core material that does not change for different operating points. The increase of energy loss per cycle in measurements on waveforms illustrated in Fig. 3(a) leads to twice ΔE, since there are two transitions to zero voltage. Consequently, in Fig. 4, the loss increase is labeled as $2 \cdot \Delta E$. Different measurements on

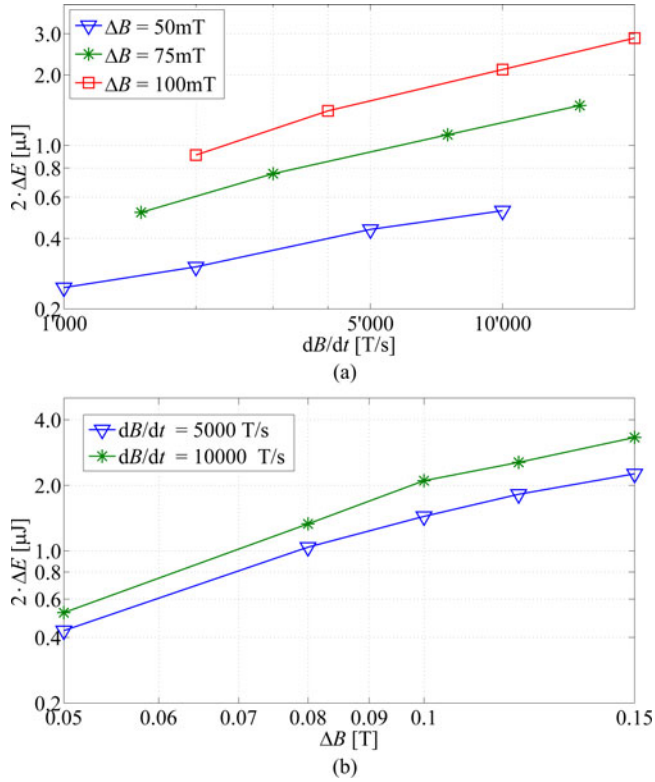

Fig. 6. Measured values of $2 \cdot \Delta E$ (ferrite N87; measured on R42 core); temperature = 25 °C.

waveforms as illustrated in Fig. 3(a) have been conducted to determine a formula to describe ΔE. The corresponding results are given in Fig. 6, where measured values of $2 \cdot \Delta E$ for different operating points are plotted. In Fig. 6(a), $\mathrm{d}B/\mathrm{d}t$ has been used as the x-axis, and in Fig. 6(b), ΔB has been chosen for the x-axis. In both cases, approximately, parallel straight lines are drawn, i.e., $2 \cdot \Delta E$ (approximately) follows a power function with variables $\mathrm{d}B/\mathrm{d}t$ and ΔB. Hence, ΔE of one transition to zero voltage can be described by a power function with variables ΔB and $\mathrm{d}B(t_-)/\mathrm{d}t$, where ΔB and $\mathrm{d}B(t_-)/\mathrm{d}t$ define the flux density waveform before this transition to zero voltage as illustrated in Fig. 7. As a consequence, the following power function can be defined for ΔE

$$\Delta E = k_\mathrm{r} \left| \frac{\mathrm{d}}{\mathrm{d}t} B(t_-) \right|^{\alpha_\mathrm{r}} (\Delta B)^{\beta_\mathrm{r}} \tag{9}$$

where α_r, β_r, and k_r are new model parameters, which have to be determined empirically. With (9), the relaxation losses of a transition to zero voltage can be determined according to the antecedent flux density slope $\mathrm{d}B(t_-)/\mathrm{d}t$ and the antecedent flux density peak-to-peak value ΔB. Accordingly, when the flux density reaches and remains at zero, as occurs, e.g., in a buck converter that is operating in discontinuous conduction mode, relaxation losses have to be taken into consideration as well. However, the losses may slightly differ in this situation because the antecedent flux density is dc biased. This dc level of the antecedent flux density has not been part of investigation of this study and could be investigated as part of future work.

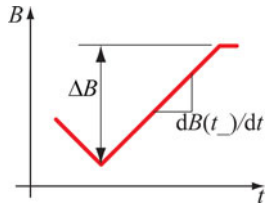

Fig. 7. Definition of $\mathrm{d}B(t_-)/\mathrm{d}t$ and ΔB.

In conclusion, (2) has been extended by an additional term that describes the loss behavior for a transient to constant flux. This leads to a new model to calculate the time-average power loss density

$$P_\mathrm{v} = \frac{1}{T}\int_0^T k_i \left|\frac{\mathrm{d}B}{\mathrm{d}t}\right|^\alpha (\Delta B)^{\beta-\alpha}\,\mathrm{d}t + \sum_{l=1}^{n} P_{\mathrm{r}l} \qquad (10)$$

where $P_{\mathrm{r}l}$ represents the time-average power loss density due to the lth of n transients to zero voltage. This power loss of each transient to zero voltage is calculated according to

$$P_{\mathrm{r}l} = \frac{1}{T} k_\mathrm{r} \left|\frac{\mathrm{d}}{\mathrm{d}t} B(t_-)\right|^{\alpha_\mathrm{r}} (\Delta B)^{\beta_\mathrm{r}} \left(1 - e^{-\frac{t_l}{\tau}}\right). \qquad (11)$$

For the sake of completeness, a limitation of the given model should be pointed out. The curves in Fig. 6 do not have the shape of exact straight lines. This illustrates the fact that the newly introduced parameters α_r and β_r are only valid for a limited $\mathrm{d}B(t_-)/\mathrm{d}t$ and ΔB range. The limited parameter validity is a general problem of the Steinmetz approach.

V. Model Derivation 2: Triangular Flux Waveform

Often in power electronics, one has a period of zero voltage applied to a magnetic component winding, e.g., in the transformer of a bidirectional isolated dc–dc converter with dual active full bridges (DABs). A DAB will be presented in Section VII as an example to illustrate the model. In this case, (10) can directly be used to improve the loss model.

However, another frequently occurring waveform is a triangular flux waveform in which the flux slope changes to another *nonzero* value. This case is illustrated in Fig. 8. When a duty cycle of 50% ($D = 0.5$) is assumed, directly after switching to the opposite voltage, the flux slope reverses, the material has hardly any time to move toward the new thermal equilibrium. As a consequence, no notable loss increase is expected, and thus, this case is well described by the iGSE (2). However, when the duty cycle goes to smaller values, once in each period, a high flux slope is followed by a very slow flux change. Assuming D to be infinitely small, a switch to a constant flux happens. Consequently, in this case, the iGSE (2) is not accurate and the relaxation term has to be added. In all operating points, where $D > 0$ and $D < 0.5$ (or $D > 0.5$ and $D < 1$), a behavior that is in between these two cases is expected. In other words, only part of the relaxation term has to be added.

In Fig. 9, the calculated and measured core losses as a function of the duty cycle are plotted. One calculation has been performed based on the iGSE (2), which, according to the previous discussion, represents the lower limit of possible losses

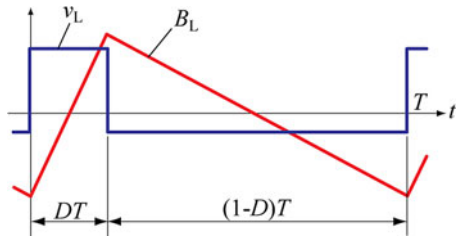

Fig. 8. Triangular flux density waveform.

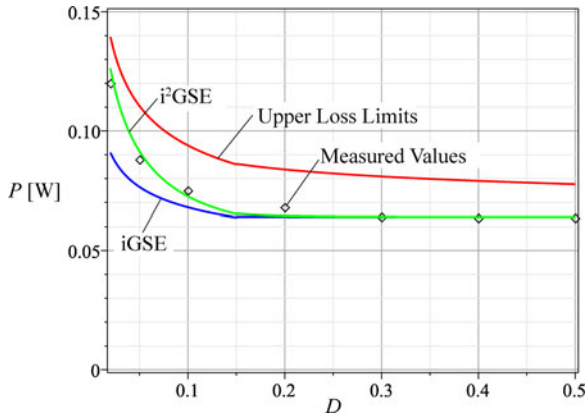

Fig. 9. Core-loss duty cycle dependence. $\Delta B = 0.1\,\mathrm{T}$, $f = 20\,\mathrm{kHz}$.

(as no relaxation effects are taken into account). It should be noted that two sets of Steinmetz parameters have been used for the calculation of the iGSE. The reason is that the Steinmetz parameters are only valid in a limited $\mathrm{d}B/\mathrm{d}t$ range, and the $\mathrm{d}B/\mathrm{d}t$ in this experiment is varying in a wide range. This explains the sharp bend of the iGSE curve at $D = 0.15$ (change of the Steinmetz parameter). Another calculation has been made always including the full relaxation loss term and which represents the upper loss limit. In other words, it can be said that losses are expected to have values between the line representing the upper loss limit and the line representing the lower loss limit (iGSE). According to the previous discussion, the real losses are closer to the lower loss limit for D close to 0.5, and losses are closer to the upper loss limit for D close to zero. Measurements seem to confirm this hypothesis as can be seen in Fig. 9. Other operating points showed the same behavior.

Based on the previous discussion, the new approach can be further improved to be also valid for triangular flux waveforms. Basically, (10) can be rewritten as

$$P_\mathrm{v} = \frac{1}{T}\int_0^T k_i \left|\frac{\mathrm{d}B}{\mathrm{d}t}\right|^\alpha (\Delta B)^{\beta-\alpha}\,\mathrm{d}t + \sum_{l=1}^{n} Q_{\mathrm{r}l} P_{\mathrm{r}l} \qquad (12)$$

where $Q_{\mathrm{r}l}$ has to be further defined. In the case of a switch to zero voltage, $Q_{\mathrm{r}l}$ needs to have the value 1. Furthermore, it has to have a structure such that (12) fits the measurement points of a duty cycle measurement, such as illustrated in Fig. 9. The following function has been chosen

$$Q_{\mathrm{r}l} = e^{-q_\mathrm{r}\left|\frac{\mathrm{d}B(t_+)/\mathrm{d}t}{\mathrm{d}B(t_-)/\mathrm{d}t}\right|} \qquad (13)$$

where $\mathrm{d}B(t_-)/\mathrm{d}t$ represents the flux density before the switching, $\mathrm{d}B(t_+)/\mathrm{d}t$ is the flux density after the switching, and q_r is a new material parameter. For a triangular waveform as illustrated in Fig. 8, (13) can be rewritten (for $D \leq 0.5$) as

$$Q_{\mathrm{r}l} = e^{-q_\mathrm{r} \frac{\frac{\Delta B}{(1-D)T}}{\frac{\Delta B}{DT}}} = e^{-q_\mathrm{r} \frac{D}{1-D}}. \tag{14}$$

In the case of the material Epcos N87, $q_\mathrm{r} = 16$ has been found; the resulting loss curve is plotted in Fig. 9. Before giving an illustrative example in Section VII, the new model will be summarized and the steps to extract the model parameters will be given.

VI. New Core-Loss Model: The i^{2}GSE

A new loss model that substantially increases the expected accuracy when core losses are modeled has been introduced. We call this new model the *improved-improved generalized Steinmetz equation* (i^{2}GSE). The name has been chosen because it is an improved version of the iGSE [4]. The time-average power loss density can be calculated with

$$P_\mathrm{v} = \frac{1}{T}\int_0^T k_i \left|\frac{\mathrm{d}B}{\mathrm{d}t}\right|^\alpha (\Delta B)^{\beta-\alpha}\,\mathrm{d}t + \sum_{l=1}^{n} Q_{\mathrm{r}l} P_{\mathrm{r}l}. \tag{15}$$

Here, $P_{\mathrm{r}l}$ is calculated for each voltage change according to

$$P_{\mathrm{r}l} = \frac{1}{T} k_\mathrm{r} \left|\frac{\mathrm{d}}{\mathrm{d}t} B(t_-)\right|^{\alpha_\mathrm{r}} (\Delta B)^{\beta_\mathrm{r}} \left(1 - e^{-\frac{t_1}{\tau}}\right). \tag{16}$$

$Q_{\mathrm{r}l}$ is a function that further describes the voltage change and is

$$Q_{\mathrm{r}l} = \mathrm{e}^{-q_\mathrm{r}\left|\frac{\mathrm{d}B(t_+)/\mathrm{d}t}{\mathrm{d}B(t_-)/\mathrm{d}t}\right|}. \tag{17}$$

α, β, k_i, α_r, β_r, k_r, τ, and q_r are the material parameters.

Now, the steps to extract the model parameters are as follows.

1) First, the parameters k_i, α, and β are extracted. The core is excited with a rectangular voltage waveform that leads to a symmetric triangular flux waveform. Measurements at three operating points are performed; then, (15) is solved for the three parameters. For symmetric triangular flux waveforms (with duty cycle D =0.5), it is $\sum_{l=1}^{n} Q_{\mathrm{r}l} P_{\mathrm{r}l} = 0$. In Table I, the measurement results and the corresponding parameters are given. These parameters could be extracted directly from the data sheet as well, as explained in [4].
2) The parameter τ can be read from Fig. 4 with
$$\frac{\Delta E}{\tau} = \frac{\mathrm{d}E}{\mathrm{d}t} \tag{18}$$
where $\mathrm{d}E/\mathrm{d}t$ represents the slope of the energy increase directly after switching to zero voltage. This is illustrated in Fig. 4. $\tau = 6\,\mu$s has been extracted for the material N87.
3) The parameters k_r, α_r, and β_r are extracted by performing measurements at three operating points with t_1 large enough to let the material reach the thermal equilibrium. Then, (9) is solved for the three parameters. In Table I, the measurement results and the corresponding parameters are given.
4) The parameter q_r has to be selected such that (15) fits the measurement points of a duty cycle measurement, as illustrated in Fig. 9.

TABLE I
Measurement Results and Model Parameter of Material EPCOS N87

Operating Point (ΔB; f)	**Loss Density** [kW/m^3]	**Model Parameters**
(0.1 T; 20 kHz)	5.98	$k_i = 8.41$
(0.1 T; 50 kHz)	16.2	$\alpha = 1.09$
(0.2 T; 50 kHz)	72.8	$\beta = 2.16$
(ΔB; $\mathrm{d}B(t_-)/\mathrm{d}t$)	[J/m^3]	
(0.1 T; 4 kT/s)	0.068	$k_\mathrm{r} = 0.0574$
(0.1 T; 20 kT/s)	0.13	$\alpha_\mathrm{r} = 0.39$
(0.2 T; 20 kT/s)	0.32	$\beta_\mathrm{r} = 1.31$
		$\tau = 6\,\mu$s
		$q_\mathrm{r} = 16$

TABLE II
Specifications of a DAB Transformer

$V_\mathrm{DC} = V_1 = V_2$	42 V
f	50 kHz
N=N_1=N_2	20
Effective Magnetic Length l_e	103 mm
Effective Magnetic Cross Section A_e	95.75 mm^2
Core	EPCOS N87, R42 (B64290L22X87) [18]

All model parameters are summarized in Table I. Extracting the parameters is sometimes difficult and measurements have to be performed very carefully. One error source is a possible current decrease due to a voltage drop over the inductor winding during "zero" voltage phase. This can be avoided by choosing a high amount of primary turns. This increases the inductance value and the current is kept more constant (by choosing a high amount of primary turns the winding copper resistance increases as well; however, the inductance value increases quadratically, while the resistance value increases linearly).

VII. Example of How to Use the New Model

In the previous section, a new core-loss modeling approach was introduced. This section shows an easy-to-follow example that illustrates how to calculate core losses of a transformer employed in a bidirectional isolated dc–dc converter with DABs [6], [21]. In Fig. 10(a), the simplified schematic, and in Table II, the specifications of the transformer are given. The shape of the core influences the core losses; however, this is not the scope of this study; hence, a simple toroid is considered as the transformer core. Phase-shift modulation has been chosen as the modulation method: the primary and secondary full bridge switches with 50% duty cycle to achieve rectangular voltages v_1 and v_2 across the primary and secondary transformer sides, respectively. The waveforms are illustrated in Fig. 10(b), including the magnetic flux density B_μ of the transformer core. A phase shift γ between v_1 and v_2 results in a power transfer. When the voltages v_1 and v_2 are opposed (which is the case in the phase t_γ), the full voltage drop is across the transformer leakage inductance and the magnetic flux density B_μ remains unchanged.

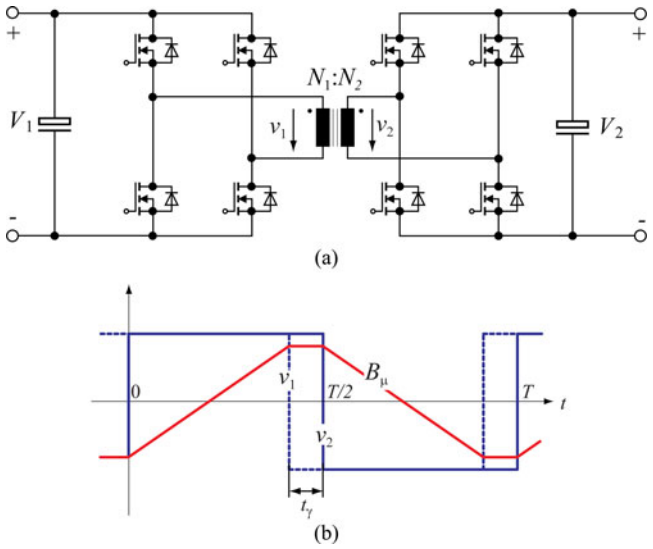

Fig. 10. (a) DAB schematic and (b) waveforms with specifications given in Table II.

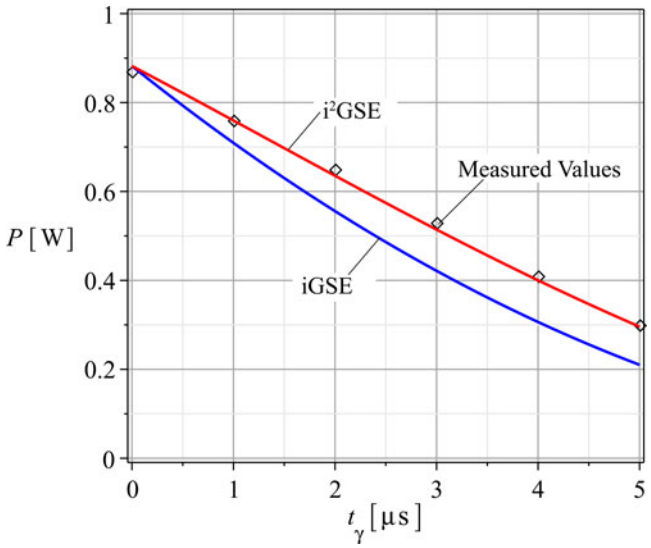

Fig. 11. Loss calculation and loss measurement comparison of the DAB example.

Only the time behavior of the magnetic flux density B_μ has been considered for designing the transformer, i.e., no winding losses or leakage inductance have been calculated. The value of the leakage inductance is very important for the functionality; however, it is not discussed here. Therefore, no statement about feasibility is made; the circuit should only represent a simple and easy-to-follow illustrative magnetic example.

The losses are calculated according to the $\mathrm{i}^2\mathrm{GSE}$ (15). The results are then compared with measurement results. The peak flux density in the core can be calculated with [6]

$$\hat{B} = \frac{1}{2}\frac{V_\mathrm{dc}}{NA_\mathrm{e}}\left(\frac{T}{2} - t_\gamma\right) \tag{19}$$

and its time derivative with

$$\frac{\mathrm{d}B}{\mathrm{d}t} = \begin{cases} \dfrac{V_\mathrm{dc}}{NA_\mathrm{e}} & \text{for } t \geq 0 \text{ and } t < \dfrac{T}{2} - t_\gamma \\ 0 & \text{for } t \geq \dfrac{T}{2} - t_\gamma \text{ and } t < \dfrac{T}{2} \\ -\dfrac{V_\mathrm{dc}}{NA_\mathrm{e}} & \text{for } t \geq \dfrac{T}{2} \text{ and } t < T - t_\gamma \\ 0 & \text{for } t \geq T - t_\gamma \text{ and } t < T. \end{cases} \tag{20}$$

Calculating the losses according to (15) leads to the following expression as a function of t_γ

$$P = \frac{T - 2t_\gamma}{T} k_i \left|\frac{V_\mathrm{dc}}{NA_\mathrm{e}}\right|^\alpha \left|\frac{V_\mathrm{dc}}{NA_\mathrm{e}}\left(\frac{T}{2} - t_\gamma\right)\right|^{\beta-\alpha} A_\mathrm{e} l_\mathrm{e} + A_\mathrm{e} l_\mathrm{e} \sum_{l=1}^{n} Q_{\mathrm{r}l} P_{\mathrm{r}l} \tag{21}$$

where $\sum_{l=1}^{2} Q_{\mathrm{r}l} P_{\mathrm{r}l}$ represents the two transients to zero voltage. There are two switching instants to zero voltage, each with $Q_{\mathrm{r}l} = 1$. The values for $P_{\mathrm{r}l}$, then, have to be determined: it is for each transient

$$P_{\mathrm{r}l} = \frac{1}{T} k_\mathrm{r} \left|\frac{V_\mathrm{dc}}{NA_\mathrm{e}}\right|^{\alpha_\mathrm{r}} \left|\frac{V_\mathrm{dc}}{NA_\mathrm{e}}\left(\frac{T}{2} - t_\gamma\right)\right|^{\beta_\mathrm{r}} \left(1 - e^{-\frac{t_\gamma}{\tau}}\right). \tag{22}$$

TABLE III
MODEL PARAMETER OF MATERIAL VITROPERM 500F (VAC)

α	1.88
β	2.02
k_i	$137 \cdot 10^{-6}$
α_r	0.76
β_r	1.70
k_r	$139 \cdot 10^{-6}$
τ	4.5 μs
q_r	4

The losses have been calculated according to the new approach and have been compared to a calculation using the classic iGSE (2) and with measurement results. Open-circuit (no-load) measurements have been performed to validate the new model: the primary winding is excited to achieve a flux density as illustrated in Fig. 10(b). Measurements for different values of t_γ have been performed, at a constant frequency f and voltage V_dc. The new model and measurement results match very well as shown in Fig. 11.

In [6], different state-of-the-art core-loss calculation approaches are compared using a very similar example. The iGSE (2) showed the best agreement with measurements, but for increasing zero-voltage periods t_γ, the calculated core losses start deviating from the measured core losses. The reason becomes clear with the new approach $\mathrm{i}^2\mathrm{GSE}$ and the calculation can be improved.

VIII. MEASUREMENTS ON DIFFERENT MATERIALS

The approach has been confirmed on different materials, including on VITROPERM 500F from VAC (measured on W452 core). Measurements on waveforms as illustrated in Fig. 3(a) have been performed. Fig. 12 shows the corresponding measurement results. The model parameters are given in Table III. Measurements show that the approach is applicable for all

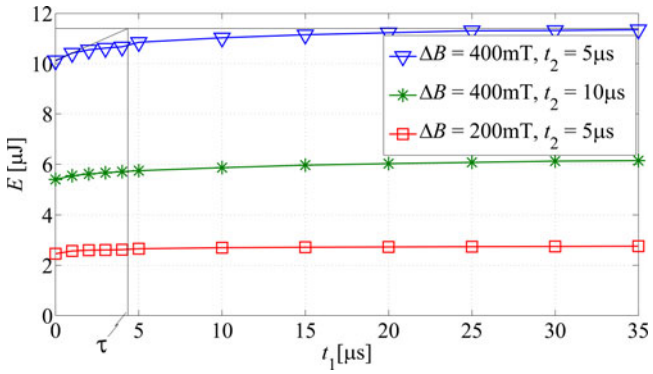

Fig. 12. Measurement results measured on VITROPERM 500F from VAC (measured on W452 core); temperature $= 25\,^{\circ}\mathrm{C}$. It is further illustrated how τ according to (18) can be extracted.

material types; however, this remains to be confirmed as part of a future work.

IX. Conclusion and Future Work

The Steinmetz equation (1) and its extension iGSE (2) are relatively accurate models for describing core losses. However, some core-loss mechanisms cannot be described with an equation of only three parameters. The Steinmetz parameters alone are insufficient to fully describe core losses. This publication together with the work presented in [17] show new approaches to how core losses can be better determined.

As experimentally verified, core losses are not necessarily zero when zero voltage is applied across a transformer or inductor winding after an interval of changing flux density. A short period after switching the winding voltage to zero, losses still occur in the material. This study hypothesizes that this is due to magnetic relaxation. A new loss modeling approach has been introduced and named $\mathrm{i}^2\mathrm{GSE}$. The $\mathrm{i}^2\mathrm{GSE}$ needs five new parameters to calculate new core-loss components. Hence, in total, eight parameters are necessary to accurately determine core losses.

The tested measurement range is given in the following to identify the range in which the model validity has been confirmed. Two types of waveforms have been analyzed: trapezoidal as illustrated in Fig. 3(a) and triangular waveforms as illustrated in Fig. 8. For trapezoidal waveforms, measurements with $t_1 = 0, \ldots, 500\ \mu\mathrm{s}$ and $t_2 = 5, \ldots, 100\ \mu\mathrm{s}$ have been conducted. For the triangular waveforms measurements in the range between 20 and 100 kHz and $D = 0.02, \ldots, 0.5$ have been conducted. No measurements for very low values of t_2 have been conducted; however, the triangular operating point with $D = 0.02$ and $f = 20\,\mathrm{kHz}$, for instance, has a flux rise time of $1\,\mu\mathrm{s}$, which indicates that the model is also applicable for very short voltage pulses.

As stated in Section I, the Steinmetz parameters are valid only for a limited frequency and flux density range. This is also the case for the additional parameters of the $\mathrm{i}^2\mathrm{GSE}$ as has been illustrated in Fig. 6; however, this parameter dependence has not been further investigated in this study. Furthermore, a dc level of the antecedent flux density has not been part of the investigation of this study and could be considered as part of a future work.

Acknowledgment

The authors would like to thank ABB Switzerland Ltd., Baden-Dättwil, Switzerland, for giving them the opportunity to work on this very interesting project.

References

[1] E. C. Snelling, *Soft Ferrites, Properties and Applications*, 2nd ed. London, U.K.: Butterworths, 1988.
[2] J. Reinert, A. Brockmeyer, and R. De Doncker, "Calculation of losses in ferro- and ferrimagnetic materials based on the modified Steinmetz equation," *IEEE Trans. Ind. Appl.*, vol. 37, no. 4, pp. 1055–1061, Jul./Aug. 2001.
[3] J. Li, T. Abdallah, and C. R. Sullivan, "Improved calculation of core loss with nonsinusoidal waveforms," in *Proc. Ind. Appl. Conf., 36th IEEE IAS Annu. Meeting*, 2001, vol. 4, pp. 2203–2210.
[4] K. Venkatachalam, C. R. Sullivan, T. Abdallah, and H. Tacca, "Accurate prediction of ferrite core loss with nonsinusoidal waveforms using only Steinmetz parameters," in *Proc. IEEE Workshop Comput. Power Electron.*, 2002, pp. 36–41.
[5] J. Biela, U. Badstuebner, and J. W. Kolar, "Impact of power density maximization on efficiency of dc–dc converter systems," *IEEE Trans. Power Electron.*, vol. 24, no. 1, pp. 288–300, Jan. 2009.
[6] I. Villar, U. Viscarret, I. Etxeberria-Otadui, and A. Rufer, "Global loss evaluation methods for nonsinusoidally fed medium-frequency power transformers," *IEEE Trans. Ind. Electron.*, vol. 56, no. 10, pp. 4132–4140, Oct. 2009.
[7] S. Iyasu, T. Shimizu, and K. Ishii, "A novel iron loss calculation method on power converters based on dynamic minor loop," in *Proc. Eur. Conf. Power Electron. Appl.*, 2005, pp. 2016–2022.
[8] T. Shimizu and K. Ishii, "An iron loss calculating method for ac filter inductors used on PWM inverters," in *Proc. 37th IEEE Power Electron. Spec. Conf.*, 2006, pp. 1–7.
[9] K. Terashima, K. Wada, T. Shimizu, T. Nakazawa, K. Ishii, and Y. Hayashi, "Evaluation of the iron loss of an inductor based on dynamic minor characteristics," in *Proc. Eur. Conf. Power Electron. Appl.*, 2007, pp. 1–8.
[10] J. B. Goodenough, "Summary of losses in magnetic materials," *IEEE Trans. Magn.*, vol. 38, no. 5, pp. 3398–3408, Sep. 2002.
[11] W. A. Roshen, "A practical, accurate and very general core loss model for nonsinusoidal waveforms," *IEEE Trans. Power Electron.*, vol. 22, no. 1, pp. 30–40, Jan. 2007.
[12] J. Liu, T. G. Wilson Jr., R. C. Wong, R. Wunderlich, and F. C. Lee, "A method for inductor core loss estimation in power factor correction applications," in *Proc. Appl. Power Electron. Conf. Expo.*, 2002, pp. 439–445.
[13] C. R. Sullivan, J. H. Harris, and E. Herbert, "Core loss predictions for general PWM waveforms from a simplified set of measured data," in *Proc. Appl. Power Electron. Conf. Expo.*, 2010, pp. 1048–1055.
[14] B. Carsten, "Why the magnetics designer should measure core loss, with a survey of loss measurement techniques and a low cost, high accuracy alternative," in *Proc. Power Electron., Intell. Motion Power Quality*, 1995, pp. 163–179.
[15] F. Dong Tan, J. Vollin, and S. Cuk, "A practical approach for magnetic core-loss characterization," *IEEE Trans. Power Electron.*, vol. 10, no. 2, pp. 124–130, Mar. 1995.
[16] W. Shen, F. Wang, D. Boroyevich, and C. W. Tipton, "Loss characterization and calculation of nanocrystalline cores for high-frequency magnetics applications," *IEEE Trans. Power Electron.*, vol. 23, no. 1, pp. 475–484, Jan. 2008.
[17] J. Mühlethaler, J. Biela, J. W. Kolar, and A. Ecklebe, "Core losses under dc bias condition based on Steinmetz parameters," in *Proc. IEEE/IEEJ Int. Power Electron. Conf. ECCE Asia*, 2010, pp. 2430–2437.
[18] *Ferrites and Accessories*, EPCOS AG, Munich, Germany, 2007.
[19] G. Bertotti, *Hysteresis in Magnetism*. New York: Academic, 1998.
[20] S. Chikazumi, *Physics of Ferromagnetism*. London, U.K.: Oxford Univ. Press, 1997.
[21] F. Krismer and J. W. Kolar, "Accurate power loss model derivation of a high-current dual active bridge converter for an automotive application," *IEEE Trans. Ind. Electron.*, vol. 57, no. 3, pp. 881–891, Mar. 2010.

Jonas Mühlethaler (S'09) received the M.Sc. degree in electrical engineering from the Swiss Federal Institute of Technology (ETH) Zurich, Zurich, Switzerland, in 2008. During his studies, he focused on power electronics and electrical machines. His M.Sc. thesis, which he wrote at ABB Corporate Research in Sweden, focused on compensating torque pulsation in permanent magnet motors. Since 2008, he has been working toward the Ph.D. degree in the Power Electronic Systems Laboratory, focusing on modeling and designing magnetic components.

Jürgen Biela (S'04–M'06) received the Diploma (Hons.) degree in electrical engineering from Friedrich-Alexander University (FAU) Erlangen, Nuremberg, Germany, in 1999 and the Ph.D. degree from the Swiss Federal Institute of Technology (ETH) Zürich, Zurich, Switzerland, in 2006, which was focused on optimized electromagnetically integrated resonant converter. During his studies, he focused in particular on resonant dc-link inverters at Strathclyde University, Glasgow, U.K., and the active control of series-connected IGCTs at the Technical University of München, Munich, Germany.

He was with the Research Department of A&D Siemens, Munich, Germany, where he worked on inverters with very high switching frequencies, SiC components, and electromagnetic compatibility. From 2006 to 2007, he was a Postdoctoral Fellow with PES and was a Guest Researcher at the Tokyo Institute of Technology, Tokyo, Japan. From 2007 to mid-2010, he was a Senior Research Associate with PES. Since August 2010, he has been the Associate Professor and Head of the Laboratory for High Power Electronic Systems at ETH Zurich. His research interests include design, modeling, and optimization of PFC, dc–dc, and multilevel converters with emphasis on SMART Grid, electric mobility and traction applications as well as pulsed-power systems for medical and accelerator applications.

Johann Walter Kolar (F'10) received the M.Sc. and Ph.D. degrees (*summa cum laude/promotio sub auspiciis praesidentis rei publicae*) from the Vienna University of Technology, Vienna, Austria. He is the Founder/Co-Founder of four spin-off companies targeting ultrahigh speed drives, multidomain/level simulation, ultracompact/efficient converter systems, and pulsed power/electronic energy processing.

Since 1984, he has been working as an independent international Consultant in close collaboration with the Vienna University of Technology, in the fields of power electronics, industrial electronics, and high-performance drives. He has proposed numerous novel converter topologies and modulation/control concepts, e.g., the VIENNA Rectifier, the Swiss Rectifier, and the three-phase ac–ac Sparse Matrix Converter. He has published more than 400 scientific papers in international journals and conference proceedings and has filed more than 80 patents. He was appointed as a Professor and the Head of the Power Electronic Systems Laboratory, Swiss Federal Institute of Technology (ETH) Zurich, Zurich, Germany, on February 1, 2001. His current research interests include ac–ac and ac–dc converter topologies with low effects on the mains, e.g., for data centers, more-electric-aircraft, and distributed renewable energy systems, and solid-state transformers for smart microgrid systems. His research interests also include the realization of ultra-compact and ultra-efficient converter modules employing the latest power semiconductor technology (SiC and GaN), micro power electronics, and/or power supply on chip systems, multidomain/scale modeling/simulation and multiobjective optimization, physical model-based lifetime prediction, pulsed power, and ultra-high speed and bearing-less motors.

Dr. Kolar received the Best Transactions Paper Award of the IEEE Industrial Electronics Society in 2005, the Best Paper Award of the International Conference on Performance Engineering in 2007, the 1st Prize Paper Award of the IEEE IAS Industrial Power Converter Committee in 2008, the IEEE Industrial Electronics Society Best Paper Award of the IES PETC in 2009, the 2009 IEEE Power Electronics Society Transaction Prize Paper Award, the 2010 Best Paper Award of the IEEE/ASME Transactions on Mechatronics, the Best Paper 1st Prize Award at the ECCE Asia 2011, and the 1st Place IEEE IAS Society Prize Paper Award 2011. He also received an Erskine Fellowship from the University of Canterbury, Canterbury, New Zealand, in 2003. In 2006, the European Power Supplies Manufacturers Association (EPSMA) awarded the Power Electronics Systems Laboratory of ETH Zurich as the Leading Academic Research Institution in Power Electronics in Europe. He is a member of the Institute of Electrical Engineers of Japan (IEEJ) and of International Steering Committees and Technical Program Committees of numerous international conferences in the field (e.g., the Director of the Power Quality Branch of the International Conference on Power Conversion and Intelligent Motion). He is the founding Chairman of the IEEE Power Electronics Society Austria and Switzerland Chapter and the Chairman of the Education Chapter of the EPE Association. From 1997 to 2000, he served as an Associate Editor of the IEEE TRANSACTIONS ON INDUSTRIAL ELECTRONICS, and since 2001, he has been an Associate Editor of the IEEE TRANSACTIONS ON POWER ELECTRONICS. Since 2002, he has also been an Associate Editor of the *Journal of Power Electronics* of the Korean Institute of Power Electronics and a Member of the Editorial Advisory Board of the *IEEJ Transactions on Electrical and Electronic Engineering*.

Andreas Ecklebe (M'07) received the Dipl.-Ing. degree in electrical engineering in 2002 and the Dr.-Ing. degree in electrical engineering in 2009 both from the Otto-von-Guericke University, Magdeburg, Germany.

From 2002 to 2004, he was with SMS Demag AG, Düsseldorf, Germany, and Alstom Power Conversion, Berlin, Germany, where he was engaged in the design of technological control systems for large-scale industrial automation solutions. Since 2008, he has been with ABB Corporate Research, Baden-Dättwil, Switzerland, where he is currently leading the Power Electronics Integration Research Group.